COBEM 2021 26th International Congress of Mechanical Engineering
November 22-26, 2021, Virtual Congress, Brazil

COB-2021-0713
SELF-SENSING ACTIVE VIBRATION CONTROL USING ELECTROMAGNETIC ACTUATORS

Beatriz Granado Marangoni
Felipe Carmo Carvalho
Marcus Vinicius Fernandes de Oliveira
Aldemir Ap Cavalini Jr.
Valder Steffen Jr.
LMEst - Structural Mechanics Laboratory, Federal University of Uberlândia, School of Mechanical Engineering, Av. João Naves de Ávila, 2121, Uberlândia, MG, 38408-196, Brazil
beatriz.marangoni@ufu.br, fcc@ufu.br, marcusfernandesss@ufu.br, aacjunior@ufu.br, vsteffen@ufu.br

Abstract. *The present work aims to apply an active vibration control (AVC) approach using electromagnetic actuators and the self-sensing methodology. The voltage and current present in the electromagnetic coils are used as a control action, thus not requiring physical displacement sensors. In this work, the mentioned control approach was applied in test rig composed of a clamped-clamped beam and two electromagnetic actuators placed in a differential configuration. The beam was mathematically represented using a one degree of freedom (DoF) mass-spring-damper system. Thus, a self-sensing proportional-integral-derivative (PID) control was analyzed for different external excitation frequencies. The obtained results demonstrated the efficiency of the conveyed approach in reducing the vibration amplitudes of the considered model. Regarding the experimental tests, a shaker was used to apply the external excitation with different frequencies applied separately in the beam within a range of interest. The purpose of these tests was to verify the behavior of the self-sensing actuator/controller set and to validate this control methodology under different conditions. Besides, a conventional proportional-derivative (PD) controller was applied using the vibration responses of the beam measured using an accelerometer. Thus, comparisons were made between the results obtained by these two control approaches. Both numerical and experimental tests demonstrated the effectiveness of the considered self-sensing control methodology.*

Keywords: *electromagnetic actuators, vibration control, mass-spring-damper, self-sensing, test rig.*

1. INTRODUCTION

Vibration control is mandatory for efficient industrial machines and equipment. Therefore, the use of rotating shafts supported by Active Magnetic Bearings (AMB) has been increasing in the last years due to its main characteristic of absence of lubrication and friction, allowing to obtain high rotation speeds without mechanical wear. Additionally, AMBs can actively control the shaft vibration amplitudes and can act as a self-diagnosis system for fault detection purposes (Maslen and Schweitzer, 2009). It is worth mentioning that AMBs are based on the attraction force generated by Electromagnetic Actuators (EMAs).

EMAs are widely studied in the literature, from their basic operating principles (electromagnetism) to parts involving optimization of their function (control). These systems are used in rotating machines for AVC purposes normally based on sensors to measure displacements and generate proportional control currents. However, self-sensing based active control approaches are being applied with EMAs.

Self-Sensing describes techniques that use EMAs as actuators and sensors. This methodology involves the mathematical model of the EMA to estimate information about the parameters associated with the control action, for instance, the position and/or force (Hanson and Levesley, 2004). This position stands for the gap between the EMA and the shaft (called air gap), which is a relevant parameter in the control action and can be estimated from the voltage and/or current measured using the self-sensing approach. Therefore, control information is obtained without any physical displacement sensor.

Vischer and Bleuler (1993), Mizuno and Bleuler (1995), Mizuno *et al.* (1996), and Noh and Maslen (1997) presented different models capable of representing the applicability of self-sensing control in AMBs. These models describe the behavior of the self-sensing control through current measurements in the coils of the bearing, a geometric approach to estimate the air gap, state observers, and a switching amplifier. Rarick (2007) explored three new vibration control techniques applied in AMBs, being these methods used to estimate the rotor position through displacement sensors and the self-sensing approach. Niemann (2008) acted in the amplitude modulation of a high frequency injected signal in the coil of a AMB. In this work, self-sensing methodologies proposed in the literature were evaluated, proposing improvements,

and investigating possible new methods.

Maslen and Schweitzer (2009) details the entire theoretical formulation, design, and applicability of AMBs used in rotating machines. The self-sensing methodology for these bearings is addressed with the mathematical formulation of the electromagnetic circuit, the control, and the technical challenges that exist for its application in the industry. Niemann *et al.* (2013) presented the direct current measurement approach for self-sensing AMBs. Therefore, the authors applied demodulation self-sensing techniques to estimate the rotor position by measuring the current ripple component. A transient simulation of the model was carried out, as well as an experimental application.

In this context, the present work aims the study the AVC approach based on self-sensing applied in a simplified system consisting of a beam clamped at its ends and two EMAs in a differential assembly. The mathematical/numerical model presented in this work was modeled according to that proposed by Rarick (2007), Maslen and Schweitzer (2009), and Niemann *et al.* (2013). The control technique used was the PID, which corresponds to a simpler and more intuitive approach. Because of this, it is most commonly used in the industrial sector.

2. TEST RIG

The test rig used in the present work is shown in Fig. 1, in which the EMAs perform self-sensing AVC by measuring the current in the coils. The test rig is composed by a clamped-clamped steel beam with dimensions 325x25x1 mm. Two EMAs were fixed near the middle of the beam on supports made in a 3D printing. Each of them is composed of two parts, being an E shaped part, called core, and an I shaped part, called target, which is coupled to the beam to drive the magnetic field generated by the control effort. In this case, measurements were performed along the horizontal direction by an accelerometer PCB Piezotronics (model 352C22) attached to the beam. However, this accelerometer was not used for vibration control purposes. A self-sensing AVC was performed by measuring the current in the EMAs coil by the oscilloscope Tektronix (model TCP A300). An electrodynamic shaker was used to apply the external excitation horizontally in the beam.

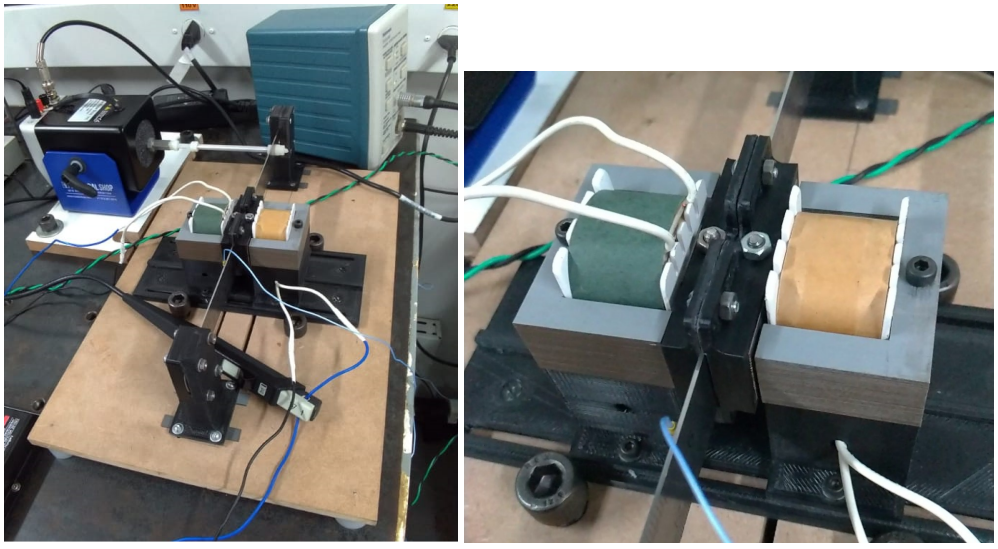

(a) Test-rig used in the self-sensing AVC. (b) EMAs used to apply the self-sensing AVC.

Figure 1. Test-rig used in the present work.

3. MATHEMATICAL MODELING

In the present work, a simplified one DoF mass-spring-damper model was used in the numerical simulations. The total mass of the test-rig was considered to obtain the value of m; the equivalent stiffness k was determined using the principles of strength of materials; and the damping c was obtained using the proportional model based on empirical constants α and β associated with the mass and stiffness of the model, respectively. Two opposite EMAs were used to perform the self-sensing AVC due to the attractive electromagnetic forces. Figure 2 presents the schematic representation of the considered model.

This model is a fundamental basis for testing the self-sensing approach to be applied in more complex systems. Some hypotheses were adopted in the analyses that will be presented next (Rarick, 2007; Chapman, 2013; Maslen and Schweitzer, 2009; Niemann *et al.*, 2013), namely: the reluctance in the circuit is contained in the air gap, leakage flux are negligible, the magnetic core material is linear (ignoring nonlinearities such as hysteresis, saturation, and the effects of eddy currents), the gap flux density is uniform, and it is assumed the one DoF system moves only along the x-direction.

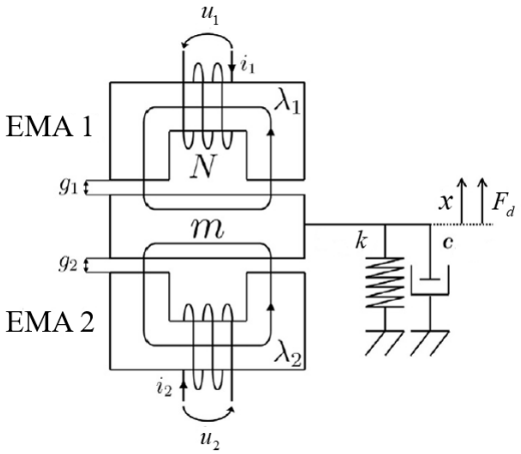

Figure 2. Simplified one DoF mass-spring-damper model.

The electromagnetic forces generated by the two EMAs in the model, F_1 and F_2, can be obtained from the magnetic flux in the air gap. The total magnetic force F is determined by energy considerations as given by Eq. (1) (Rarick, 2007; Bonfitto *et al.*, 2017).

$$F = \frac{1}{\mu_0 A_g}\left(\mu_0 N A_g \frac{i}{2g}\right) = \frac{K}{4}\frac{i^2}{g^2} \tag{1}$$

where μ_0 is the permeability of the air gap, A_g is the cross-sectional area of the air gap, N is the number of turns in the coil, i is the current in the coil, and g is the air gap length (K is associated with the EMA parameters).

Therefore, the equation of motion for the model considered in this work (see Fig. 2) is presented in Eq. (3).

$$m\ddot{x} + c\dot{x} + kx = F_1 - F_2 + F_d \tag{2}$$

$$m\ddot{x} + c\dot{x} + kx = \frac{K}{4}\left(\frac{i_1}{g_1}\right)^2 - \frac{K}{4}\left(\frac{i_2}{g_2}\right)^2 + F_d \tag{3}$$

where F_d is a disturbance force.

The electromagnetic coils of EMAs can be modeled as a RL electrical circuit (resistive-inductive circuits) with the presence of an back-EMF induced in the coil. From Kirchoff's Law and Faraday's Law, the total voltage in the coil circuits can be represented as given by Eq. (4) (Rarick, 2007; Maslen and Schweitzer, 2009; Bonfitto *et al.*, 2017).

$$u = iR + L_s\frac{\mathrm{d}i}{\mathrm{d}t} + \frac{K}{2}\frac{\mathrm{d}}{\mathrm{d}t}\left(\frac{i}{g}\right) \tag{4}$$

where u is the total voltage in the coil, R is the coil resistance, and L_s is the coil self-inductance. Therefore, the voltage in each EMA is presented in Eq. (5) and Eq. (6).

$$u_1 = i_1 R + L_{s1}\frac{\mathrm{d}i_1}{\mathrm{d}t} + \frac{K}{2}\frac{\mathrm{d}}{\mathrm{d}t}\left(\frac{i_1}{g_1}\right) \tag{5}$$

$$u_2 = i_2 R + L_{s1}\frac{\mathrm{d}i_2}{\mathrm{d}t} + \frac{K}{2}\frac{\mathrm{d}}{\mathrm{d}t}\left(\frac{i_2}{g_2}\right) \tag{6}$$

Therefore, the EMAs model presents two inputs (u_1 and u_2) and four outputs, namely g_1, g_2, i_1, and i_2; although for the application of self-sensing control only the currents are required. The air gap lengths of the EMAs are given by Eq. (7).

$$g_1 = x_0 - x \quad g_2 = x_0 + x \tag{7}$$

where x_0 is the nominal air gap and x is the position of the mass m (see Fig. 2).

The states of this nonlinear system can be represented by the vector defined in Eq. (8) (Rarick, 2007; Niemann, 2008).

$$z = \begin{bmatrix} z_1 \\ z_2 \\ z_3 \\ z_4 \end{bmatrix} = \begin{bmatrix} x \\ \dot{x} \\ i_1 \\ i_2 \end{bmatrix} \tag{8}$$

From Eq. (3) to Eq. (6), the nonlinear states of the model are determined as follows:

$$z = f(z, u, F_d) = \begin{bmatrix} z_2 \\ -\frac{k}{m}z_1 + \frac{K}{4m}\left(\frac{z_3}{g_0 - z_1}\right)^2 - \frac{K}{4m}\left(\frac{z_4}{g_0 - z_1}\right)^2 - \frac{c}{m}z_2 + \frac{1}{m}F_d \\ \frac{2(g_0 - z_1)}{2L_s(g_0 - z_1) + K}\left[-Rz_3 - \frac{K}{2(g_0 - z_1)^2}z_2 z_3 + u_1\right] \\ \frac{2(g_0 + z_1)}{2L_s(g_0 + z_1) + K}\left[-Rz_4 + \frac{K}{2(g_0 + z_1)^2}z_2 z_4 + u_2\right] \end{bmatrix} \tag{9}$$

The dynamic behavior of the system can be linearized around its operating point (beam at rest; z_0, i_0, F_{d0}) by applying the Jacobian transformation. In the operating point, a bias current i_0 and resistance R are imposed for both actuators; and there is no initial disturbance force (F_{d0}) (Rarick, 2007; Niemann, 2008; Bonfitto *et al.*, 2017). Thus, the following state space model is obtained:

$$\dot{z} = Az + B_1 u + B_2 F_d \tag{10}$$

$$A = \begin{bmatrix} 0 & 1 & 0 & 0 \\ \frac{Ki_0^2}{mg_0^3} - \frac{k}{m} & -\frac{c}{m} & \frac{Ki_0}{2mg_0^2} & -\frac{Ki_0}{2mg_0^2} \\ 0 & -\frac{Ki_0}{g_0(K + 2g_0L_s)} & -\frac{2g_0R}{K + 2g_0L_s} & 0 \\ 0 & \frac{Ki_0}{g_0(K + 2g_0L_s)} & 0 & -\frac{2g_0R}{K + 2g_0L_s} \end{bmatrix} \tag{11}$$

$$B_1 = \begin{bmatrix} 0 & 0 \\ 0 & 0 \\ \frac{2g_0}{K + 2g_0L_s} & 0 \\ 0 & \frac{2g_0}{K + 2g_0L_s} \end{bmatrix} \tag{12}$$

$$B_2 = \begin{bmatrix} 0 \\ \frac{1}{m} \\ 0 \\ 0 \end{bmatrix} \tag{13}$$

Thus, the linearized matrices are given by Eq. (14).

$$A = \begin{bmatrix} 0 & 1 & 0 & 0 \\ \frac{2k_x}{m} - \frac{k}{m} & -\frac{c}{m} & \frac{k_i}{m} & -\frac{k_i}{m} \\ 0 & -\frac{k_i}{L} & -\frac{R}{L} & 0 \\ 0 & \frac{k_i}{L} & 0 & -\frac{R}{L} \end{bmatrix}, B_1 = \begin{bmatrix} 0 & 0 \\ 0 & 0 \\ \frac{1}{L} & 0 \\ 0 & \frac{1}{L} \end{bmatrix}, B_2 = \begin{bmatrix} 0 \\ \frac{1}{m} \\ 0 \\ 0 \end{bmatrix} \tag{14}$$

where,

$$k_x = \frac{Ki_0^2}{2g_0^3}, \qquad k_i = \frac{Ki_0}{2g_0^2}, \qquad L = \frac{K + 2g_0L_s}{2g_0} \tag{15}$$

$$\frac{Ki_0}{g_0(K + 2g_0L_s)} = \frac{Ki_0}{2g_0^2}\frac{2g_0}{K + 2g_0L_s} = \frac{k_i}{L} \tag{16}$$

where k_i is the current-force factor and k_x is the force-displacement factor or negative stiffness of one EMA.

4. CONTROL DESIGN

The present section aims to describe the design strategy of a PID self-sensing AVC in the considered beam. This controller is calculated in the time domain from the feedback error $e(t)$, as shown in Eq. (17). The numerical model of the control approach implemented in this work is based on the K_p, K_I, and K_D gains. However, only the proportional (K_p) and derivative (K_D) gains were used in the experimental tests. In this case, the beam is clamped at its ends, not presenting steady-state error (corrected by K_I). The derivative gain K_D represents an additional damping in the system control.

$$u(t) = K_p e(t) + K_I \int e(t) + K_p \frac{\mathrm{d}e}{\mathrm{d}t} \tag{17}$$

The PD controller input was the voltage measured at one of the EMAs. The outputs were the control currents, which were applied with a phase delay of 180 degrees in the EMA 1 and EMA 2. Figure 3 illustrates the logic adopted in the experimental tests.

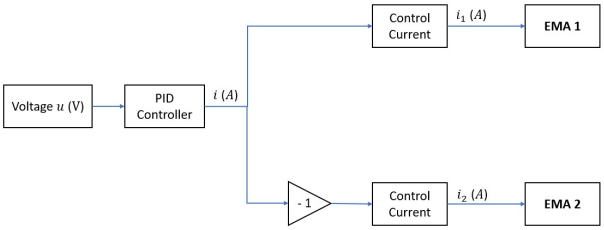

Figure 3. Logic used to generate the voltage-based control currents.

In the numerical modeling, the control loop for the self-sensing PID controller was designed using the voltage of only one EMA as the output signal. The PID controller was powered by the error signal from the reference signal and the acquired voltage signal. This controller then calculates the current required to stabilize the system, which is applied to the EMAs. However, this control current is added to a bias current. Furthermore, the considered model is also influenced by an external force. The representation of this control system is shown in Fig. 4. The optimal gains for the numerical model were calculated by the PID Tuner code available in Matlab/Simulink®, wich automatically determines the best gains from the nominal values of the linearized model.

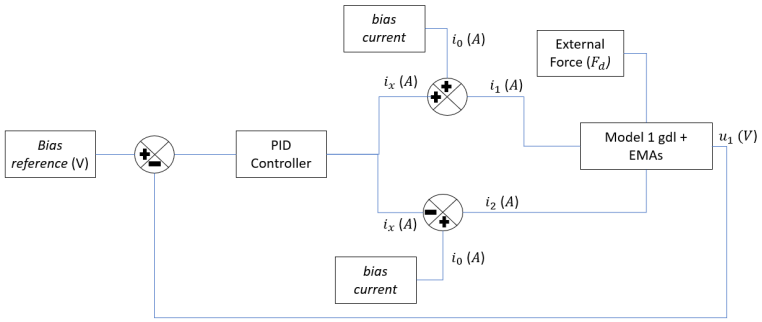

Figure 4. Numeric model control loop.

The experimental self-sensing PD vibration control loop uses the current signal in the EMAs circuit (current converted into voltage). From this aim, a block diagram were developed in Matlab/Simulink routine in communication with the dSPACE board for performing the control on the test-rig (see Fig. 5). The determination of the proportional and derivative gains of the self-sensing PD control in the experimental tests was carried out by observing the behavior of the beam displacement for different gain values (trial and error approach). Thus, the selected gains (resulted in the smallest vibration amplitude of the system) for each excitation frequency.

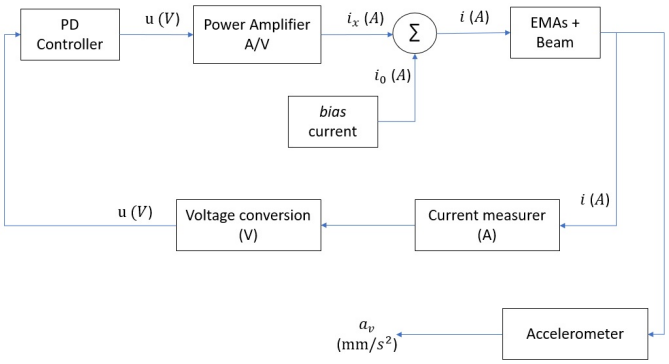

Figure 5. Block diagram for performing self-sensing PD control on the test-rig.

5. NUMERICAL AND EXPERIMENTAL RESULTS

Table (1) presents the parameters used in the numerical model to obtain the results of the self-sensing PID control.

Table 1. Mechanical, electrical, and magnetic parameters used in the numerical model.

Parameters	**Values**
Mass [kg]	1.927
Stiffness [N/m]	$2.821\text{x}10^{9}$
Structural Damping [N.s/m]	30.138
Permeability of the air gap [H/m]	$4\pi\text{x}10^{-7}$
Cross-Sectional Area [m^2]	$1.948\text{x}10^{-4}$
Number of turns	250
Bias Current [A]	1
Resistence [Ω]	1.17
Inductance EMA 1 [mH]	32.1
Inductance EMA 2 [mH]	29.3
Nominal Air Gap [m]	$4\text{x}10^{-3}$
Current-force factor [N/A]	46.346
Force-displacement factor [N/m]	$1.179\text{x}10^{5}$

Numerical simulations were performed for different external excitation frequencies based on the control strategy illustrated in Fig. 4. Int his case, the following gains were adopted: $k_p = 0.3747$, $k_I = 293.9336$, and $k_D = -2.2696x10^{-4}$ (calculated by the PID Tuner code). Figure 6 shows the obtained numerical results. It is worth mentioning that the natural frequency (f_n) of the mechanical system is $60.9Hz$.

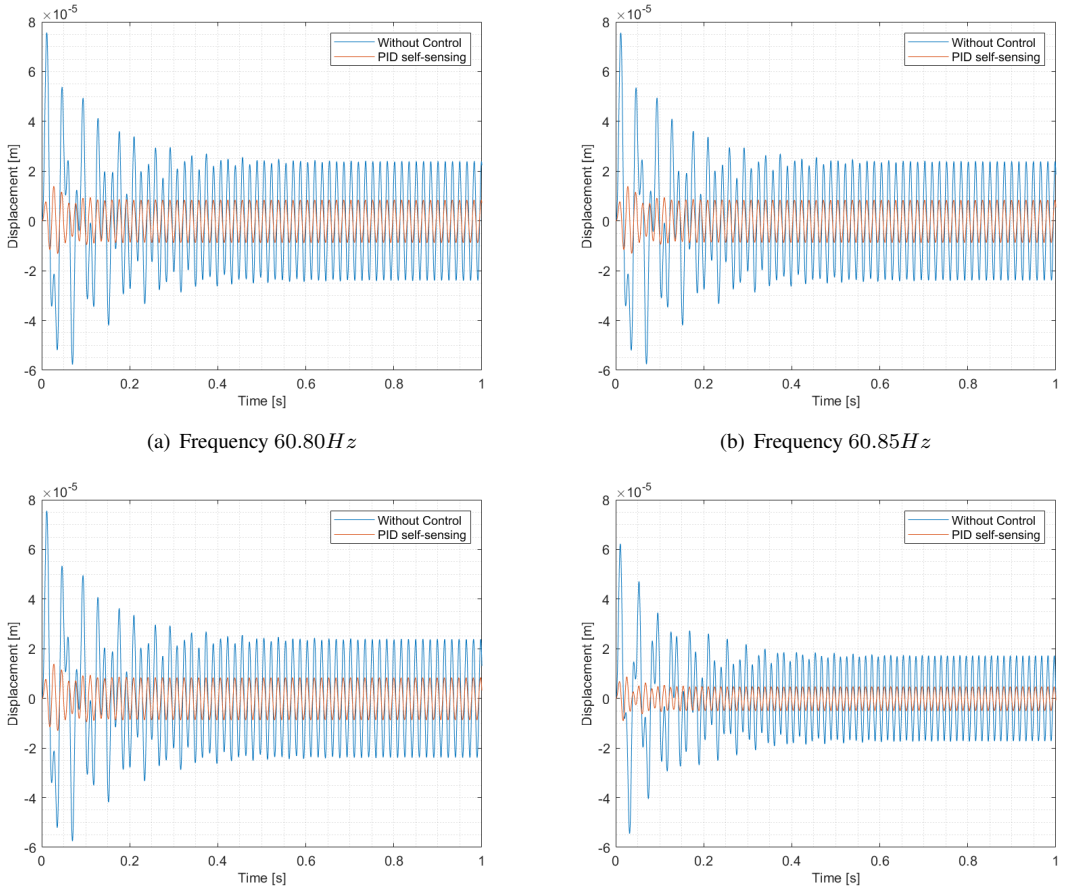

(a) Frequency $60.80Hz$ (b) Frequency $60.85Hz$

(c) Frequency $60.90Hz$ (d) Frequency $70.00Hz$

Figure 6. Numerical time domain vibration responses: — without control; — PID self-sensing control.

Note that the self-sensing PID vibration control approach was able to reduce the vibration amplitude of the system in all tested external excitation frequencies. Table (2) shows the reductions achieved in the vibration amplitudes of the system, which demonstrates the numerical effectiveness of the presented self-sensing AVC strategy.

Table 2. Numerical vibration reductions.

Excitation frequency [Hz]	**Reduction %]**
60.80	64.82
60.85	64.87
60.90	64.85
70.00	72.73

In the experimental tests, a bias current of 0.1 A was used only to keep the EMAs energized. It was observed during the tests that high bias values caused an overheating of the actuator, impairing the self-sensing PD control action. The length of the air gap was $1.0mm$. Each experiment was performed during $20s$ (the sampling time used for data acquisition purposes was 5.10^{-4} s).

Figure 7 presents the experimental results obtained in the time domain applying the self-sensing approach. The accelerometer was used in this application only to evaluate the efficiency of the self-sensing AVC approach. The Fast Fourier Transforms (FFTs) of these vibration responses are presented in Fig. 8. The experimental tests were performed considering different external excitation frequencies, all close to the first natural frequency of the experimental test-rig (27.25 Hz).

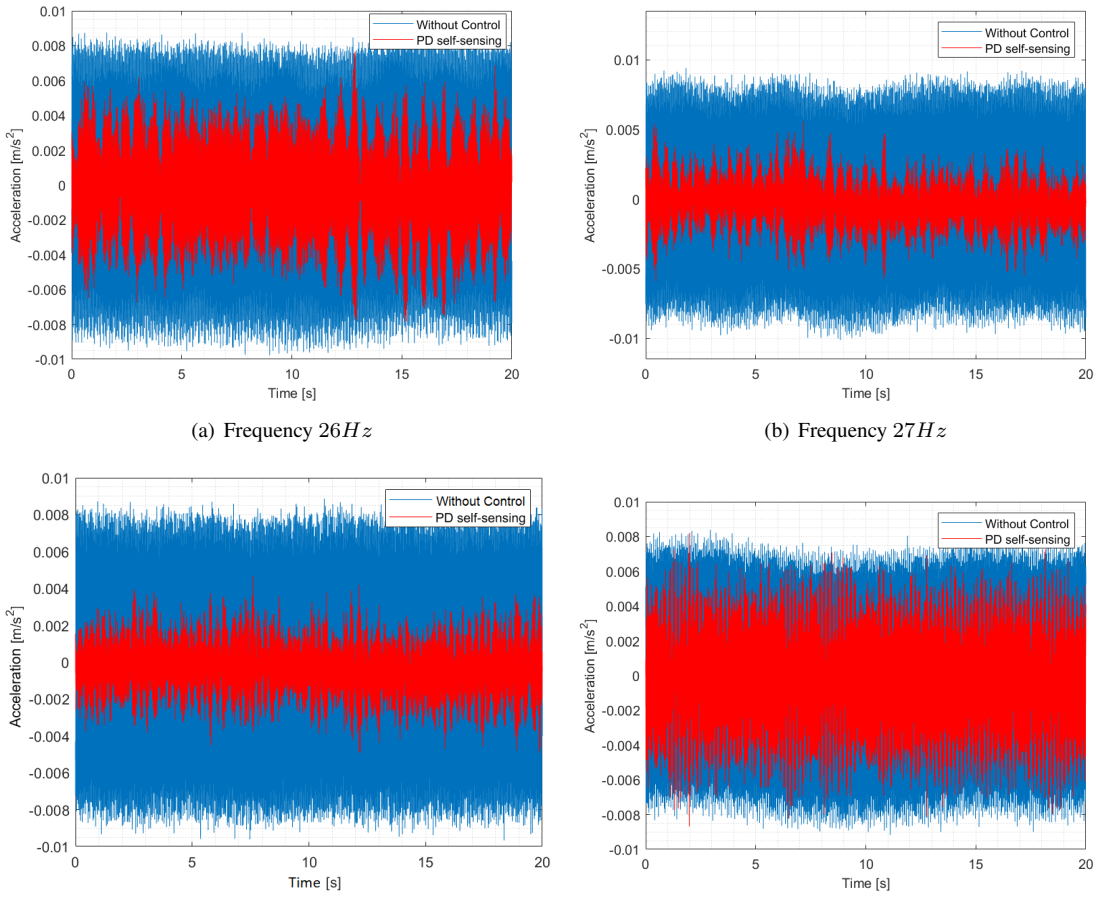

(a) Frequency $26Hz$ (b) Frequency $27Hz$

(c) Frequency $28Hz$ (d) Frequency $30Hz$

Figure 7. Experimental time domain vibration responses: — without control; — PID self-sensing control.

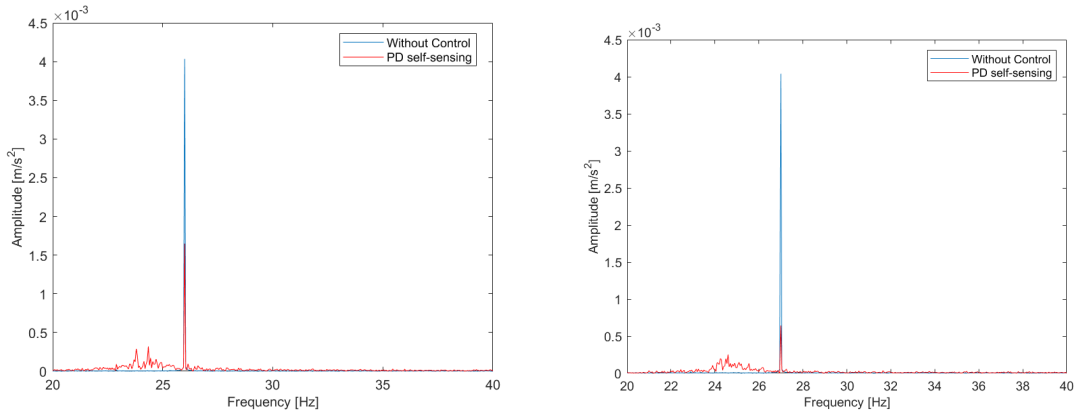

(a) Frequency $26Hz$ (b) Frequency $27Hz$

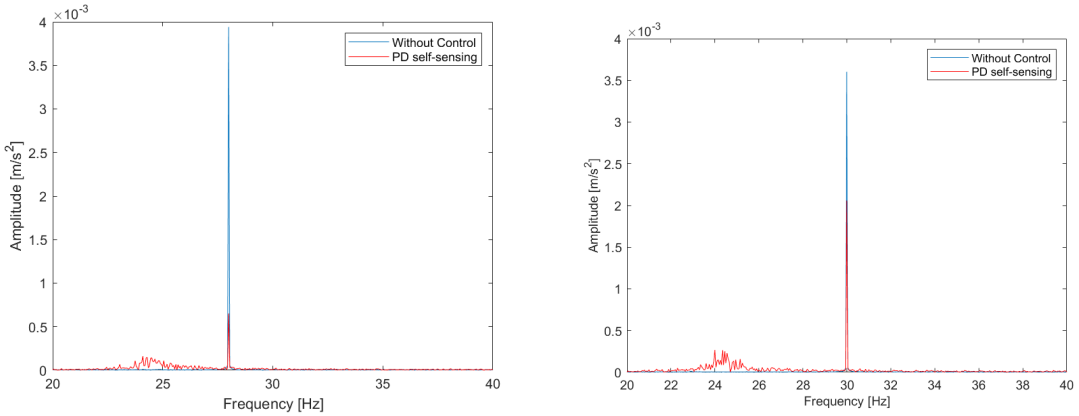

(c) Frequency $28Hz$ (d) Frequency $30Hz$

Figure 8. Experimental frequency domain vibration responses: — without control; — PID self-sensing control.

According to the results of the experimental tests, it is noticed that the self-sensing PD control reduced the vibration of the beam satisfactorily. It can also be observed that the vibration reduction was greater for frequencies close to the first natural frequency of the test-rig. Therefore, the self-sensing controller presented efficient results in the range of interest for the test rig considered in this study. Table (3) shows the reductions achieved in the experimental vibration amplitudes of the system.

Table 3. Experimental vibration reductions.

Excitation frequency [Hz]	**Reduction [%]**
26	49.28
27	74.58
28	71.43
30	51.59

6. FINAL REMARKS

This work aimed to develop a self-sensing AVC approach applied in a simplified system (mass-spring-damper) consisting of a clamped-clamped beam and two diametrically arranged EMAs. For this purpose, a literature review was carried out on the most common self-sensing methodologies, concluding that the most suitable for the application of this work was the PID controller. Numerical and experimental analyses were carried out to verify the effectiveness of the self-sensing AVC approach considered in the present contribution. The obtained results demonstrated the effectiveness of the evaluated technique, reducing the vibration amplitude of the system more than 60% and 49% in the numerical and experimental tests, respectively. Further research effort will be dedicated to apply the conveyed methodology in a rotor supported by AMBs.

7. ACKNOWLEDGEMENTS

The authors are thankful for the financial support provided to the present research effort by CNPq (43431337/2018-7, 3062000/2017-1 and 305958/2020-8), FAPEMIG, CAPES through the INCT-EIE, and Petrobras.

8. REFERENCES

Bonfitto, A., Tonoli, A. and Silvagni, M., 2017. "Sensorless active magnetic dampers for the control of rotors". *Mechatronics*, Vol. 47, pp. 195–207.

Chapman, S.J., 2013. *Fundamentos de máquinas elétricas*. AMGH editora.

Hanson, B. and Levesley, M., 2004. "Self-sensing applications for electromagnetic actuators". *Sensors and Actuators A: Physical*, Vol. 116, No. 2, pp. 345–351.

Maslen, E.H. and Schweitzer, G., 2009. *Magnetic bearings: theory, design, and application to rotating machinery*. Springer.

Mizuno, T. and Bleuler, H., 1995. "Self-sensing magnetic bearing control system design using the geometric approach". *Control Engineering Practice*, Vol. 3, No. 7, pp. 925–932.

Mizuno, T., Araki, K. and Bleuler, H., 1996. "Stability analysis of self-sensing magnetic bearing controllers". *IEEE transactions on control systems technology*, Vol. 4, No. 5, pp. 572–579.

Niemann, A.C., Van Schoor, G. and Du Rand, C.P., 2013. "A self-sensing active magnetic bearing based on a direct current measurement approach". *Sensors*, Vol. 13, No. 9, pp. 12149–12165.

Niemann, A.C., 2008. *Self-sensing algorithms for active magnetic bearings*. Ph.D. thesis, North-West University.

Noh, M.D. and Maslen, E.H., 1997. "Self-sensing magnetic bearings using parameter estimation". *IEEE Transactions on Instrumentation and Measurement*, Vol. 46, No. 1, pp. 45–50.

Rarick, R.A., 2007. *Control of an active magnetic bearing with and without position sensing*. Ph.D. thesis, Cleveland State University.

Vischer, D. and Bleuler, H., 1993. "Self-sensing active magnetic levitation". *IEEE Transactions on Magnetics*, Vol. 29, No. 2, pp. 1276–1281.